

---

# OR-NeRF: Object Removing from 3D Scenes Guided by Multiview Segmentation with Neural Radiance Fields

---

**Youtan Yin\***

Nanyang Technological University  
youtan001@e.ntu.edu.sg

**Zhoujie Fu\***

Nanyang Technological University  
zhoujie001@e.ntu.edu.sg

**Fan Yang**

Nanyang Technological University  
fan007@e.ntu.edu.sg

**Guosheng Lin<sup>†</sup>**

Nanyang Technological University  
gslin@ntu.edu.sg

## Abstract

The emergence of Neural Radiance Fields (NeRF) for novel view synthesis has led to increased interest in 3D scene editing. One important task in editing is removing objects from a scene while ensuring visual reasonability and multiview consistency. However, current methods face challenges such as time-consuming object labelling, limited capability to remove specific targets, and compromised rendering quality after removal. This paper proposes a novel object-removing pipeline, named OR-NeRF, that can remove objects from 3D scenes with either **point** or **text** prompts on a **single** view, achieving better performance in less time than previous works. Our method uses a points projection strategy to rapidly spread user annotations to all views, significantly reducing the processing burden. This algorithm allows us to leverage the recent 2D segmentation model Segment-Anything (SAM) to predict masks with improved precision and efficiency. Additionally, we obtain colour and depth priors through 2D inpainting methods. Finally, our algorithm employs depth supervision and perceptual loss for scene reconstruction to maintain consistency in geometry and appearance after object removal. Experimental results demonstrate that our method achieves better editing quality with less time than previous works, considering both quality and quantity.

## 1 Introduction

Neural Radiance Fields (NeRF) [27] has demonstrated excellent results in reconstructing 3D scenes, and recent works [30, 46, 51, 45, 48] have aimed to extend its capabilities to editing 3D scenes. One of the essential editing operations is removing objects from a 3D scene, which has garnered significant interest from the research community [47, 44, 43, 29, 9]. However, the practical application of this task faces several challenges. One of the most significant obstacles is the accurate localization of unwanted objects. Although it is natural for humans to identify unwanted objects, asking users to label every view is impractical. Additionally, ensuring multiview consistency and plausible content after deletion without any ground truth is not trivial.

Several works have tried to address the above problems but remain unsatisfactory. Object-NeRF [47] and ObjectSDF [44] decompose the NeRF [27] training into background and objects branches,

---

\*equal contribution

<sup>†</sup>Corresponding author

allowing them to render specified objects controlled by object ID. However, because of the lack of supervision for the removed part, neither of these works [47, 44] can guarantee a plausible completion at the removal area. Weder et al. [43] and SPIn-NeRF [29] use the 2D inpainting method [38] to generate colour and depth priors after deletion and reconstruct NeRF [27] from these priors directly. Although editing quality has improved, Weder et al. [43] require all views’ masks to realize, while SPIn-NeRF [29] uses a series of segmentation preliminaries [10, 3, 55, 54] which even involves network training to generate masks for each scene with intensive time. DFFs [17] applies pre-trained language models [32, 3] to enable text-prompt editing by training NeRF [27] to align feature vectors extracted from language models [32, 3], eliminating the need for masks. However, it has difficulty locating regions to remove if the pre-trained object detector [32, 3] does not work appropriately.

In this paper, we propose a novel pipeline called OR-NeRF that enables free object removal from 3D scenes using either points or text prompts on a single image, requiring less time for multiview segmentation and achieving better performance than previous methods. To spread the points prompt on a single view to other views, we introduce a point projection strategy that utilizes the COLMAP [35] sparse reconstruction to find correspondences from 2D points to 3D sparse point cloud and further projects 3D points to all 2D images with camera parameters. This results in precise sparse points annotations for all scene views, which can be directly input to a recent 2D segmentation model Segment-Anything (SAM) [16] to predict masks. Generated at a speed of approximately two frames per second, our algorithm outperforms previous works like SPIn-NeRF [29] requiring minutes. Following the approach of Weder et al. [43] and SPIn-NeRF [29], we use the 2D inpainting model LaMa [38] to get colour priors for the removal area. We develop our scene object removal algorithm using TensoRF [4] as the backbone with depth supervision and perceptual loss. TensoRF [4] is a SOTA model for improving rendering quality considering time and performance trade-offs. This approach enables us to reconstruct the 3D scene after object removal with superior editing quality compared to existing methods. Fig 1 shows an overview of our OR-NeRF framework.

We evaluate our method on various datasets and analyze its performance in multiview segmentation and scene object removal through quality and quantity analyses. In summary, our contributions are (1) A novel pipeline for efficient object removal from 3D scenes, allowing for both points and text prompts on a single image; and (2) Experimental results demonstrate that our method achieves better editing quality and requires less time for multiview segmentation than previous methods, as evidenced by both quality and quantity analyses.

## 2 Related Work

**Multiview Segmentation** Though segmentation in 2D is well studied, multiview segmentation for 3D scenes has received less attention despite its non-negligible importance for downstream applications like 3D editing. Several self-supervised methods [7, 24] have been proposed, but they often produce inaccurate masks and have difficulty handling complex scenes. To mitigate these challenges, semi-supervised strategies [40, 8, 54, 29] have emerged that require partial annotations, or reasonable prompts from users. Semantic NeRF [54] propagates partial labels to dense semantic segmentation by leveraging a few in-place annotations via predicting semantic labels with volume rendering. Similar to NeRF [27], SPIn-NeRF [29] further constructs a thorough pipeline to generate masks for all views with points prompt on a single image. They [29] use one-shot segmentation [10] to estimate an initial mask, followed by a video segmentation [3, 38] to generate masks for all views by treating the image sequence as a video. Finally, they [29] use Semantic NeRF [54] to refine the masks. However, the above approaches require network training, which consumes considerable resources and does not guarantee an accurate mask, as errors can accumulate with complicated frameworks.

**Scene Object Removal** NeRF [27] has greatly facilitated the area of 3D scene editing, and research [1, 2, 25, 36] focuses on various editing types emerging in large numbers. Works exist for texture editing [5, 45], geometry editing [30, 46, 51], and object-centred editing [34, 50, 9, 44, 47], such as removal [21, 43, 29], and even enabling multiple manipulations [19, 17, 41, 23, 57, 49, 28, 18]. [44, 47] decompose NeRF [27] training into background and object branches, allowing for rendering specified objects controlled by assigned object IDs. However, they generate ‘black holes’ at the removal region as there is no supervision or priors for the deletion part during training. [21, 43, 29] utilize the 2D inpainting method [38] to obtain priors for the removal part and directly reconstruct

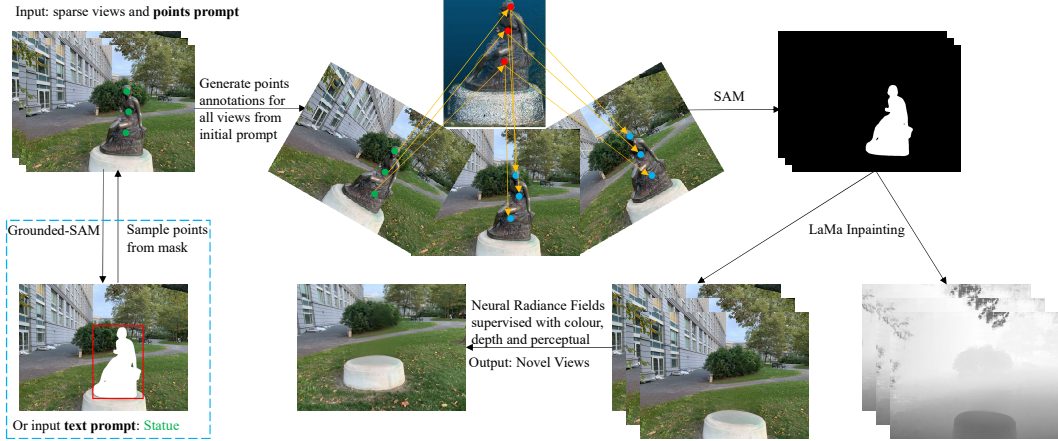


Figure 1: An overview of our OR-NeRF’s framework. We start with a set of sparse images and either points or text prompts. If a text prompt is used, we convert it into a points prompt by sampling points from the initial mask estimated using Grounded-SAM [13] (Sec 4.1.2). Next, we propagate the points annotations to all views by projecting them from 2D to 3D point cloud and then back to 2D (Sec 4.1.1). We utilize SAM [16] to predict masks using these points annotations. And LaMa is used [38] to obtain colour and depth priors. Finally, the scene after removal is reconstructed using Neural Radiance Fields supervised by colour (Eq (3)), depth (Eq (5)), and perceptual (Eq (6)) cues simultaneously (Sec 4.2).

the scene after deletion from these priors. Though achieving better rendering quality, these methods demand high preconditions, such as annotating or generating masks for all views, which rely on expensive time costs and hardware resources. Additionally, [17, 28, 9] combine pre-trained language models [3, 32, 20, 39] to enable text editing, thus bypassing the requirement for masks. Still, the rendering quality in the removal region is poor, as no algorithms are designed for learning pixel values after deletion.

### 3 Background

#### 3.1 Neural Radiance Fields

Given 3D location  $\mathbf{x} = (x, y, z)$  and 2D viewing direction  $\mathbf{d} = (\theta, \phi)$ , NeRF [27] models the 3D scene implicitly with an MLP network which gives a mapping function  $F_\Theta : (\mathbf{x}, \mathbf{d}) \rightarrow (\mathbf{c}, \sigma)$ . The output  $\mathbf{c}$  stands for the radiance and  $\sigma$  for volume density at this point, respectively. To optimize weights  $\Theta$ , the volume rendering approach [15] is introduced as:

$$C(\mathbf{r}) = \int_{t_n}^{t_f} T(t) \sigma(\mathbf{r}(t)) \mathbf{c}(\mathbf{r}(t), \mathbf{d}) dt, \text{ where } T(t) = \exp \left( - \int_{t_n}^t \sigma(\mathbf{r}(s)) ds \right). \quad (1)$$

In Eq (1),  $C(\mathbf{r})$  represents the pixel value and is calculated by integrating the radiance value  $\mathbf{c}$  along the ray  $\mathbf{r}(t) = \mathbf{o} + t\mathbf{d}$  starting from the camera position  $\mathbf{o}$  with direction  $\mathbf{d}$  pointing to the pixel, within near and far bounds  $t_n$  and  $t_f$ . The function  $T(t)$  denotes the accumulated transmittance along the ray from  $t_n$  to  $t$ . With the above definitions, NeRF [27] trains the network by minimizing the total squared error between rendered pixels and ground truth.

#### 3.2 SPIn-NeRF

SPIn-NeRF [29] proposes a comprehensive pipeline for removing objects from 3D scenes. In addition to a set of sparse view images with their corresponding camera parameters, SPIn-NeRF [29] takes a few points on one view annotated by users indicating the unwanted objects as a prompt. With these inputs, SPIn-NeRF [29] first combines a series of segmentation methods [10, 3, 55, 54] to obtain masks for all views. Then a 2D image inpainting model [38] is used to generate colour and depth priors in the mask area. The scene after deletion can be reconstructed with a modified version of

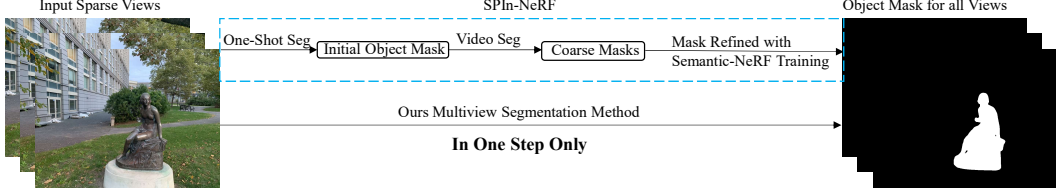


Figure 2: Comparison of mask generation between SPIn-NeRF [29] (first row) and ours (second row). Our method achieves rapid and precise mask generation for all views in a single step, supporting both points and text input. In contrast, SPIn-NeRF [29] exhibits slower speed, lower accuracy, and limited support for points prompt only, requiring three steps, including network training.

vanilla NeRF [27] from these priors directly, which adds depth supervision [6] and perceptual loss [14] to constrain the geometry and appearance consistency across different views.

In the mask generation stage, an initial mask from the single-view annotation is obtained using the one-shot segmentation [10] method. The video segmentation approach [55, 3] that follows provides coarse masks for all views by wrapping images into a video sequence. Finally, the coarse masks are fine-tuned to generate proper masks for all views by fitting the Semantic NeRF [54]. This procedure even requires training the Semantic NeRF [54] from scratch to refine coarse masks obtained from [55, 3], resulting in significant costs in terms of time and hardware. Fig 2 shows the difference in mask generation between our pipeline and SPIn-NeRF [29].

## 4 Method

Considering a set of sparse-view images with their corresponding camera poses waiting to be edited, our method requires users to provide either points or text prompts indicating the unwanted objects for only one image. Possible prompts can be a few points marked on the object or words describing the target. To begin with, we find the masks of unwanted objects in all images. We spread the initial points prompts to all images for points input according to 3D geometry match relationships (Sec 4.1.1). While for text input, we first acquire Grounded-SAM [13] to make an initial mask for the annotated single view and followed by sampling points in this initial mask to switch text prompts to the points-prompt pattern (Sec 4.1.2).

To continue, we utilize the SAM model [16] to predict masks with points prompt and use masks to guide a 2D inpainting model LaMa [38] to generate colour and depth priors. Finally, we describe our object-removing strategy guaranteeing geometry and appearance consistency across all the views (Sec 4.2). Fig 1 shows an overview of our framework for removing objects from 3D scenes with points or text prompts.

### 4.1 Multiview Segmentation

#### 4.1.1 Points Prompt

Suppose we have a group of  $n$  images  $\mathcal{I} = \{I_i\}_{i=1}^n$  and their corresponding camera parameters  $\mathcal{C} = \{C_i\}_{i=1}^n$  gathered from a 3D scene. We aim to predict masks for all views  $\mathcal{I}$  from only one-shot annotation. An intuitive approach to this question is to generate annotations for other images. We carefully investigate the 3D geometry matching relation in 3D scenes and find that a 2D point on a certain perspective can be spread to other views by projecting it back to 3D space and then projecting the corresponding 3D point to 2D planes under a certain camera pose. For 2D to 3D pass, we can refer to the sparse point cloud reconstructed by COLMAP [35] and its projected discrete points group  $\mathcal{D} = \{D_i\}_{i=1}^n$  on all 2D images. Actually, this information is represented by a certain data structure in COLMAP's [35] sparse reconstruction as a unique one-to-one mapping, which allows us to locate points in 3D space by simply querying with 2D coordinates (More details about the data structure are provided in the supplementary material). However, this introduces a new problem: finding a mapping for the user's arbitrary input is not guaranteed as the reconstruction is sparse. We can solve this question by making a query with the existing nearest points in the discrete points set  $\mathcal{D}$ . And finally, for the 3D to 2D reverse pass, we reproject 3D points back to the 2D plane under a certain view through its corresponding camera matrices. Now we can spread the initial annotation provided by users to all other views safely and quickly as this algorithm utilizes 3D information, which is

self-consistent and does not involve any neural network training. Only matrices computation is needed, and the algorithm can achieve a speed of about two frames per second for generating masks.

Specifically, we leverage the 3D geometry correspondence to calculate all views' annotation  $\mathcal{P}_{2d} = \{P_{ij}\}_{i=1}^n \}_{j=1}^m$  from the only prompt  $P_1$  provided by users and here  $P_{ij} = (x_{ij}, y_{ij})$ , while  $m$  stands for the number of points marked in an image. With  $\mathcal{P}_{2d}$ , we can obtain masks  $\mathcal{M} = \{M_i\}_{i=1}^n$  for all views easily from SAM model [16]  $\mathcal{F}_S$  by making inferences as  $\mathcal{M} = \mathcal{F}_S(\mathcal{I}, \mathcal{P}_{2d})$ . To realise this, we first initialise  $M_1$  with  $\mathcal{F}_S(I_1, P_1)$ . Then we acquire points  $\mathcal{P}_{3d} = \{(x_k, y_k, z_k)\}_{k=1}^l$  in 3D space by querying 2D coordinates  $D_1^* = (M_1 \cap D_1)$ . Note  $l$  equals the number of points in  $D_1^*$  and we only refer to the points belonging to the mask  $M_1$  as we need to constrain the points annotation for all views precisely match the unwanted objects. In practice, the nearest points are calculated after 3D points have been projected to 2D planes to ensure the amount and quality of prompts (See supplementary materials for detailed analysis).

Considering the 3D to 2D situation, we begin with camera parameters. For each view  $I_i$ , the associated camera parameters  $C_i = \{\mathbf{K}_i, \mathbf{P}_i\}$  is composed of the intrinsics  $\mathbf{K}$  and extrinsics  $\mathbf{P} = [\mathbf{R}|\mathbf{t}]$ . Here, the extrinsic matrix  $\mathbf{P}$  is represented by a  $3 \times 3$  rotation matrix  $\mathbf{R}$  (camera orientation) and a  $3 \times 1$  translation vector  $\mathbf{t}$  (camera position) that together transform the 3D point from the world coordinate system  $P_w = [X_w, Y_w, Z_w]^T$  to the camera coordinate system  $P_c = [X_c, Y_c, Z_c]^T = \mathbf{R}P_w + \mathbf{t}$ . By substituting  $\mathcal{P}_{3d}$  to  $P_w$ , we can switch 3D points  $\mathcal{P}_{3d}$  from the world coordinate system to camera coordinate system for all views simply as  $\mathcal{P}_{3d}^* = \{(x_{ik}, y_{ik}, z_{ik})\}_{i=1}^n \}_{k=1}^l = \mathbf{R}_i \mathcal{P}_{3d} + \mathbf{t}_i$ . Here  $\mathcal{P}_{3d}^*$  denotes the camera coordinate system form. And with one little step forward:

$$\mathcal{P}_{2d}^* = \{P_{ik}\}_{i=1}^n \}_{k=1}^l = \{x_{ik}/z_{ik}, y_{ik}/z_{ik}\}_{i=1}^n \}_{k=1}^l, \text{ where } (x, y, z) \in \mathcal{P}_{3d}^*, \quad (2)$$

we project 3D points  $\mathcal{P}_{3d}^*$  back to all 2D views to get corresponding pixel coordinates  $\mathcal{P}_{2d}^*$  in images. Now we need to filter the number of points in each image from  $k$  to  $m$ . To handle this issue, we spread the initial annotation  $P_1$  to all views by performing the above 2D-3D-2D projection to  $D_1^*$  similarly to get a  $\mathcal{P}'_{2d} = \{P'_{ij}\}_{i=1}^n \}_{j=1}^m$  and find the  $m$  nearest points to  $\mathcal{P}'_{2d}$  in  $\mathcal{P}_{2d}^*$  to construct  $\mathcal{P}_{2d}$ . We keep the number of points the same as the user input in each view to ensure mask quality (More details in supplementary materials). By far, we get all the annotations required for the prediction of SAM [16], and we can gain masks for all views by calling  $\mathcal{M} = \mathcal{F}_S(\mathcal{I}, \mathcal{P}_{2d})$ .

#### 4.1.2 Text Prompt

For the text prompt, we leverage SAM's [16] variety Grounded-SAM [13] which combines an object detector Grounding DINO [22] who can handle text input. A natural way to deal with text is by asking Grounded-SAM [13] to predict all the views' masks with the same text input. However, we observe a considerable speed drop in inference when comparing Grounding DINO [22] to SAM [16] (See supplementary materials for quantitative evidence). Meanwhile, Grounded-SAM [13] can fail to handle some 'difficult' views due to Grounding DINO's [22] limited detection ability. Therefore, we consider a two-stage strategy where we first use Grounded-SAM [13] to obtain an initial mask for the single view and then sample points from this mask. Finally, we use the points prompt method in Sec 4.1.1 to generate masks for the remaining views. This design ensures high-quality masks while minimizing computational costs.

Regarding  $m$  words  $\mathcal{T} = \{T_j\}_{j=1}^m$  input from the user that describe the unwanted objects. For input words sequence  $\mathcal{T}$  and images  $\mathcal{I}$  pairs, Grounding DINO [22] model  $\mathcal{F}_G$  takes the prompt  $\mathcal{T}$  as labels and tries to find these labels' corresponding bounding boxes  $\mathcal{B} = \{B_{ij}\}_{i=1}^n \}_{j=1}^m$  in images  $\mathcal{I}$  as  $\mathcal{B} = \mathcal{F}_G(\mathcal{I}, \mathcal{T})$ . As SAM [16] is capable of two kinds of inputs: points or boxes, we can obtain the mask  $M_1$  of unwanted objects in the user's annotated image  $I_1$  simply by forwarding SAM [16] with  $M_1 = \mathcal{F}_S(I_1, B_1)$ . With the one-shot mask  $M_1$ , we sample a set of  $k$  points  $\hat{\mathcal{P}} = \{P_k = (x_k, y_k)\}_{k=1}^q$  from this mask to make the problem solvable by the points prompt method (Sec 4.1.1). To implement this, we traverse the points in the mask from left to right and up to down and choose the top left, bottom right point and centre point of the mask to construct the points prompt  $\hat{\mathcal{P}}$ . Then, text prompt input has been converted into points prompt, and we let the algorithm used for points prompt in Sec 4.1.1 generate masks for all views.

## 4.2 Scene Object Removal

Once we get object masks for all views, we can reconstruct a 3D scene without unwanted objects through Neural Radiance Fields by treating 2D inpainting priors as ground truth. Recall Sec 3.1, the network can be optimized by minimizing the colour loss:

$$\mathcal{L}_c = \sum_{\mathbf{r} \in \mathcal{R}} \|\hat{C}(\mathbf{r}) - C(\mathbf{r})\|_2^2, \quad (3)$$

where  $\mathcal{R}$  is the set of rays in each training batch,  $\hat{C}(\mathbf{r})$  are the ground truth and  $C(\mathbf{r})$  are the rendered pixels by network outputs calculated through Eq (1), respectively.

However, relying solely on colour loss is inadequate, as LaMa [38] does not consider the 3D context, leading to inconsistency across different views. To address this issue, we introduce depth constraints [6] into the training of Neural Radiance Fields. Depth values  $D(\mathbf{r})$  can be obtained through volume rendering easily as:

$$D(\mathbf{r}) = \int_{t_n}^{t_f} T(t) \sigma(\mathbf{r}(t)) z dt, \text{ where } T(t) = \exp \left( - \int_{t_n}^t \sigma(\mathbf{r}(s)) ds \right). \quad (4)$$

where  $z$  is the distance from the current 3D location to the camera position. Like RGB images, we render depth images for the original scene without deletion and use LaMa [38] to get depth priors. Then, we add depth supervision to training as:

$$\mathcal{L}_d = \sum_{\mathbf{r} \in \mathcal{R}} \|\hat{D}(\mathbf{r}) - D(\mathbf{r})\|_2^2, \quad (5)$$

where  $\hat{D}(\mathbf{r})$  are the depth ground truth. We further discuss the difference between using the whole-depth image as supervision and only querying the depth in the mask area in Sec 5.3.

In addition, we recognize that depth supervision alone only enforces geometric consistency across views, while the appearance may still exhibit inconsistency. To address this, we incorporate perceptual loss [14] to guide the network in learning a plausible colour distribution within the masked region, matching the style of the inpainted colour priors. We focus the perceptual loss [14] specifically on the masked area. This is because colour loss alone is sufficient for the non-masked area, as pixel values do not change after the deletion in this area. It is important to note that the perceptual loss is designed at the image level. In our implementation, we refer to the patch-level implementation from SPIn-NeRF [29], represented by the following equation:

$$\mathcal{L}_p = \frac{1}{B} \sum_{\mathbf{i} \in \mathcal{B}} \text{LPIPS}(\hat{I}(\mathbf{r}), I(\mathbf{r})), \text{ where } I(\mathbf{r}) = \sum_{\mathbf{r} \in \mathcal{P}} C(\mathbf{r}), \quad (6)$$

and adjust the patch sampling strategy (See supplementary materials) to fit a variety of data used in our Experiments (Sec 5). In Equation (6), we first sample a patch  $\mathcal{P}$  from the mask and calculate the mean square error between the rendered pixels  $I(\mathbf{r})$  and the ground truth  $\hat{I}(\mathbf{r})$  for the pixels within the patch  $\mathcal{P}$ . Batch training with a size of  $B$  can be employed. Finally, the training objective is to minimize the total loss  $\mathcal{L}$  defined as:

$$\mathcal{L} = a * \mathcal{L}_c + b * \mathcal{L}_d + c * \mathcal{L}_p, \quad (7)$$

where  $a$ ,  $b$ , and  $c$  are tunable loss weights for the colour, depth, and perceptual loss, respectively.

## 5 Experiments

**Datasets** We select 12 scenes from various commonly used 3D reconstruction datasets, including NeRF [27] LLFF data, IBRNet data [42], and LLFF real-world data [26]. Our scene selection aims to cover a wide range of scene variations and different types of removal operations (See supplementary materials for examples. Our method allows for removing multiple objects and partial objects like slogans, providing a high degree of flexibility). Since the reconstruction datasets do not provide ground truth for evaluation, we incorporate the SPIn-NeRF [29] dataset, which includes human-annotated object masks and captures of the scene after object removal. We use all 10 scenes from the SPIn-NeRF [29] dataset to evaluate the quality of multiview segmentation. To evaluate scene object removal’s performance, we select 8 scenes, excluding two duplicate scenes, to ensure a diverse layout of the objects. To conclude, we conduct experiments on 20 scenes, comprehensively evaluating our OR-NeRF pipeline.

**Metrics** We adopt the evaluation metrics commonly used in segmentation tasks, including pixel-wise accuracy (Acc) and intersection over union (IoU), to assess the performance of our multiview segmentation algorithm. We report peak signal-to-noise ratio (PSNR), a widely used 3D reconstruction metric for the scene object removal component. Additionally, we include two metrics used by SPIIn-NeRF [29]: the learned perceptual image patch similarity (LPIPS) [53] and the Fréchet inception distance (FID) [12]. These metrics compare the similarity between the ground-truth data and the rendering outputs produced by our method.

### 5.1 Experiments Settings

**Multiview Segmentation** We conduct experiments using points and text prompts on our selected scenes and evaluate the results using metrics stated in Sec 5. Since the implementation details of multiview segmentation were not explicitly provided in the SPIIn-NeRF [29] paper, we directly utilize the metrics mentioned in their paper. However, it should be noted that the paper does not specify which scenes were used for calculating these metrics. Therefore, we compare the performance of SPIIn-NeRF [29] with our scene-average results. Subsequently, we utilize the masks generated from the points prompt for all subsequent experiments.

**Scene Object Removal** We conduct experiments on all 20 scenes with ours and the SPIIn-NeRF [29] methods. Both vanilla NeRF [27] and TensoRF [4] architectures are tested with our method’s implementation. TensoRF [4] is a current SOTA model focusing on improving rendering quality. We follow the implementation of the SPIIn-NeRF [29] to reproduce their results. For NeRF [27] and TensoRF [4], we train the original scenes to render depth maps instead of disparity maps used in SPIIn-NeRF [29]. This decision is made to avoid errors that may arise from dividing by zero when calculating disparities.

### 5.2 Multiview Segmentation

Table 1: Comparison of mask generation between our method and SPIIn-NeRF [29]. The first row indicates the scene name in the SPIIn-NeRF dataset, while ‘points’ and ‘text’ denote the prompts mode used, respectively.

	1	2	3	4	7	9	10	12	trash	Mean	SPIIn-NeRF[29]
points	acc↑	99.80	99.82	99.73	99.79	99.81	99.78	99.87	99.30	99.51	99.71↑
	IoU↑	96.77	96.47	97.48	98.50	97.43	96.29	95.47	91.73	88.68	95.42↑
text	acc↑	99.81	99.82	99.73	99.80	99.81	99.78	99.86	99.25	99.51	99.71↑
	IoU↑	96.81	96.51	97.47	98.51	97.43	96.41	95.41	91.19	88.64	95.38↑

**Quantity** Table 1 compares mask generation between our method and SPIIn-NeRF [29]. Our approach outperforms SPIIn-NeRF [29] regarding accuracy and IoU. SPIIn-NeRF’s [29] mask generation process involves a complex pipeline that introduces errors at each step and requires significant time and hardware resources. In contrast, our method leverages the simplicity of SAM [16] and involves minimal matrix calculations. Consequently, our multiview segmentation algorithm delivers superior-quality results in less time. Table 2 shows our estimated time for mask generation compared to SPIIn-NeRF [29].

Table 2: Comparison of time consumption between our method and SPIIn-NeRF [29]. Statics for SPIIn-NeRF is borrowed from their paper directly.

	One-shot Seg	Video Seg	Semantic NeRF Train	Semantic NeRF predict	2D Inpainting	Reconstruct
SPIIn-NeRF	< 1 second	< 1 minute	2-5 minutes	1 minute	< 1 minute	20-40 minutes
Ours			1 minute		<1 minute	20-40minutes

**Quality** Note that we have excluded the ‘book’ scene from the average calculation. This decision was made because we have identified inaccuracies in the ground truth labels for this particular scene, as evident from Fig 3. Furthermore, as depicted in Fig 3, our segmentation results exhibit precise coverage of the target objects with intricate details, such as the crossing chair legs in the ‘12’ scene. However, it should be noted that there is a minor flaw in the ‘trash’ scene where our masks fail to cover all areas of the trash cans explaining the low metrics in Table 1. We assert that this issue does

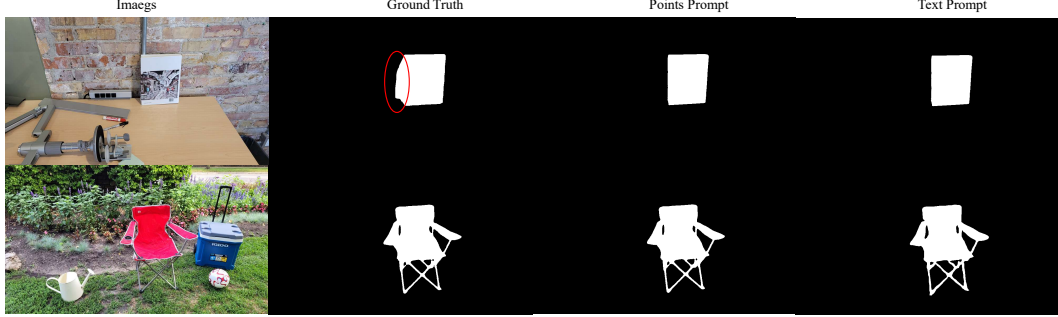


Figure 3: Mask generation results of our OR-NeRF. The figure shows the masks generated for two scenes: 'book' (up) and '12' (below) from the SPIn-NeRF [29] dataset.

not significantly affect the subsequent experiments if refined with our strategy (See details about the reason and solution in supplementary materials).

### 5.3 Scene Object Removal

Table 3: Experiment results on scene object removal. The first row indicates methods name, while abbreviations in the second row indicate loss modules. 'dir' denotes training Neural Radiance Fields with LaMa [38] priors directly, 'dp' denotes partial depth, 'da' denotes all depth, and 'lips' denotes the use of perceptual loss. Notably, perceptual loss is always applied with all-depth supervision enabled.

	Ours-NeRF[27]				Ours-TensoRF[4]			SPIn-NeRF[29]		
	dir	dp	da	lips	dir	da	lips	dir	da	lips
PSNR↑	14.04	14.04	14.16	14.16	13.93	14.04	14.03	<b>14.85</b>	14.82	14.83
FID↓	61.11	65.21	64.71	58.15	<b>53.28</b>	64.29	59.74	70.02	70.07	67.26
LPIPS↓	0.6834	0.6893	0.7022	0.6763	0.6370	0.6494	<b>0.6273</b>	0.6810	0.6752	0.6506

**Quantity** Table 3 presents our results for scene object removal. In terms of overall rendering quality, Ours-NeRF exhibits a superior FID compared to SPIn-NeRF [29] but performs worse in terms of PSNR and LPIPS. On the other hand, Ours-TensoRF outperforms SPIn-NeRF in terms of FID and LPIPS scores but has a weakness in PSNR. Analyzing the impact of the loss models, it appears that the additional components for training Neural Radiance Fields do not have a significantly positive effect. Ours-NeRF and ours-TensoRF exhibit a similar pattern where depth supervision and perceptual loss increase PSNR but show no positive influence on FID and LPIPS. Interestingly, SPIn-NeRF behaves somewhat differently: removing perceptual loss and depth supervision from the SPIn-NeRF pipeline results in a subtle increase in PSNR compared to the original version. However, the FID and LPIPS scores demonstrate that the add-ons improve SPIn-NeRF performance. While the results involve complex numbers, we adopt Ours-TensoRF with perceptual loss as it performs best overall. Although Table 3 does not provide strong evidence for the efficacy of depth supervision and perceptual loss, we will discuss the real significance of these add-ons in the following section.



Figure 4: Comparison of overall rendering quality between SPIn-NeRF (left) and Ours-TensoRF (right). We can see blurry from SPIn-NeRF compared with our clear details.

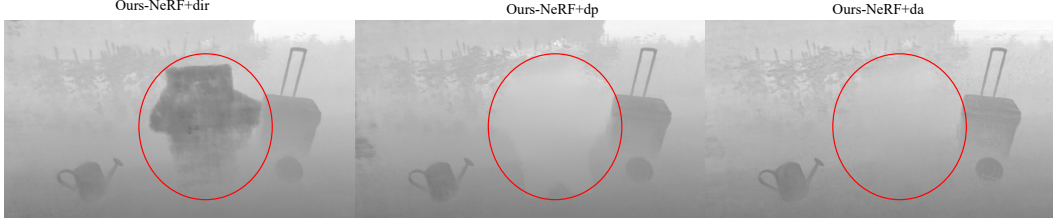


Figure 5: The effect of depth supervision. We can see from the figure that either without depth supervision (left) or training with partial depth (middle) leads to geometry inconsistency. While supervised by all-depth images (right) convergent to a consistent result.



Figure 6: The effect of perceptual loss. Left is Ours-TensoRF trained directly, and right is Ours-TensoRF with perceptual loss. We can see from the figure that this loss has some influence but is still unsatisfactory.

**Quality** We first compare the three methods’ overall rendering quality in this part. Ours-NeRF and Ours-TensoRF produce clear outputs, while SPIn-NeRF [29] suffers from blurry due to the noisy disparity maps, which provide inaccurate geometry supervision. This can be observed by Fig 4.

Next, we discuss the impact of depth supervision. Although widely used in training, there is a lack of exploration of the difference between using the entire depth image as supervision and only applying depth loss in the masked area. Fig 5 indicates that full-depth supervision is necessary and irreplaceable, as both partial depth and direct training settings in all three architectures produce inconsistent depth results, resulting in different extents of restoring removed objects. However, it is worth noting that the depth loss does not show a visible difference in the rendered views, which aligns with the metrics presented in Table 3.

Moving on to the perceptual loss aspect, we conclude from Fig 6 that this loss has a positive effect but falls short of guaranteeing a plausible completion for the masked area. This also explains the relatively ineffective metrics in Table 3, as all of our results exhibit a significant gap with the ground truth. Finally, part of our editing results are displayed in Fig 7, and more details can be found in supplementary materials.

## 6 Conclusions and Discussions

This paper presents a novel pipeline OR-NeRF for object removal from 3D scenes, requiring only points or text prompts on a single view. We emphasize the advantages of our method in terms of rendering quality and time efficiency. We also suggest that potential enhancements could incorporate more robust 2D image inpainting techniques, such as diffusion [52, 11, 33, 31, 56, 37], to achieve plausible completions after object removal.



Figure 7: Editing results of OR-NeRF demonstrating various examples. Please zoom in to observe better. More detailed experiment results can be found in the supplementary materials.

## References

- [1] Chong Bao, Yinda Zhang, Bangbang Yang, Tianxing Fan, Zesong Yang, Hujun Bao, Guofeng Zhang, and Zhaopeng Cui. SINE: Semantic-driven Image-based NeRF Editing with Prior-guided Editing Field, 2023. URL <http://arxiv.org/abs/2303.13277>.
- [2] Sagie Benaim, Frederik Warburg, Peter Ebert Christensen, and Serge Belongie. Volumetric Disentanglement for 3D Scene Manipulation, 2022. URL <http://arxiv.org/abs/2206.02776>.
- [3] Mathilde Caron, Hugo Touvron, Ishan Misra, Hervé Jegou, Julien Mairal, Piotr Bojanowski, and Armand Joulin. Emerging Properties in Self-Supervised Vision Transformers. In *2021 IEEE/CVF International Conference on Computer Vision (ICCV)*, pages 9630–9640, 2021. doi: 10.1109/ICCV48922.2021.00951.
- [4] Anpei Chen, Zexiang Xu, Andreas Geiger, Jingyi Yu, and Hao Su. TensoRF: Tensorial Radiance Fields. In *Computer Vision – ECCV 2022: 17th European Conference, Tel Aviv, Israel, October 23–27, 2022, Proceedings, Part XXXII*, pages 333–350, 2022. ISBN 978-3-031-19823-6. doi: 10.1007/978-3-031-19824-3\_20. URL [https://doi.org/10.1007/978-3-031-19824-3\\_20](https://doi.org/10.1007/978-3-031-19824-3_20).
- [5] Zhiqin Chen, Kangxue Yin, and Sanja Fidler. AUV-Net: Learning Aligned UV Maps for Texture Transfer and Synthesis. In *2022 IEEE/CVF Conference on Computer Vision and Pattern Recognition (CVPR)*, pages 1455–1464, 2022. doi: 10.1109/CVPR52688.2022.00152.
- [6] Kangle Deng, Andrew Liu, Jun-Yan Zhu, and Deva Ramanan. Depth-supervised NeRF: Fewer Views and Faster Training for Free. In *2022 IEEE/CVF Conference on Computer Vision and Pattern Recognition (CVPR)*, pages 12872–12881, 2022. doi: 10.1109/CVPR52688.2022.01254.
- [7] Zhiwen Fan, Peihao Wang, Yifan Jiang, Xinyu Gong, Dejia Xu, and Zhangyang Wang. NeRF-SOS: Any-View Self-supervised Object Segmentation on Complex Scenes, 2022. URL <http://arxiv.org/abs/2209.08776>.
- [8] Xiao Fu, Shangzhan Zhang, Tianrun Chen, Yichong Lu, Lanyun Zhu, Xiaowei Zhou, Andreas Geiger, and Yiyi Liao. Panoptic NeRF: 3D-to-2D Label Transfer for Panoptic Urban Scene Segmentation, 2022. URL <http://arxiv.org/abs/2203.15224>.
- [9] Rahul Goel, Dhawal Sirikonda, Saurabh Saini, and P. J. Narayanan. Interactive Segmentation of Radiance Fields, 2023. URL <http://arxiv.org/abs/2212.13545>.

[10] Yuying Hao, Yi Liu, Zewu Wu, Lin Han, Yizhou Chen, Guowei Chen, Lutao Chu, Shiyu Tang, Zhiliang Yu, Zeyu Chen, and Baohua Lai. EdgeFlow: Achieving Practical Interactive Segmentation with Edge-Guided Flow. In *2021 IEEE/CVF International Conference on Computer Vision Workshops (ICCVW)*, pages 1551–1560, 2021. doi: 10.1109/ICCVW54120.2021.00180.

[11] Ayaan Haque, Matthew Tancik, Alexei A. Efros, Aleksander Holynski, and Angjoo Kanazawa. Instruct-NeRF2NeRF: Editing 3D Scenes with Instructions, 2023. URL <http://arxiv.org/abs/2303.12789>.

[12] Martin Heusel, Hubert Ramsauer, Thomas Unterthiner, Bernhard Nessler, and Sepp Hochreiter. GANs trained by a two time-scale update rule converge to a local nash equilibrium. In *Proceedings of the 31st International Conference on Neural Information Processing Systems, NIPS’17*, pages 6629–6640, 2017. ISBN 978-1-5108-6096-4.

[13] IDEA-Research. Grounded-sam. <https://github.com/IDEA-Research/Grounded-Segment-Anything>, 2023.

[14] Justin Johnson, Alexandre Alahi, and Li Fei-Fei. Perceptual losses for real-time style transfer and super-resolution. In Bastian Leibe, Jiri Matas, Nicu Sebe, and Max Welling, editors, *Computer Vision – ECCV 2016*, pages 694–711, 2016. ISBN 978-3-319-46475-6.

[15] James T. Kajiya and Brian P Von Herzen. Ray tracing volume densities. *SIGGRAPH Comput Graph.*, 18(3):165–174, jan 1984. ISSN 0097-8930. doi: 10.1145/964965.808594. URL <https://doi.org/10.1145/964965.808594>.

[16] Alexander Kirillov, Eric Mintun, Nikhila Ravi, Hanzi Mao, Chloe Rolland, Laura Gustafson, Tete Xiao, Spencer Whitehead, Alexander C. Berg, Wan-Yen Lo, Piotr Dollár, and Ross Girshick. Segment Anything, 2023. URL <http://arxiv.org/abs/2304.02643>.

[17] Sosuke Kobayashi, Eiichi Matsumoto, and Vincent Sitzmann. Decomposing NeRF for Editing via Feature Field Distillation. In S. Koyejo, S. Mohamed, A. Agarwal, D. Belgrave, K. Cho, and A. Oh, editors, *Advances in Neural Information Processing Systems*, volume 35, pages 23311–23330, 2022. URL [https://proceedings.neurips.cc/paper\\_files/paper/2022/file/93f250215e4889119807b6fac3a57aec-Paper-Conference.pdf](https://proceedings.neurips.cc/paper_files/paper/2022/file/93f250215e4889119807b6fac3a57aec-Paper-Conference.pdf).

[18] Zhengfei Kuang, Fujun Luan, Sai Bi, Zhixin Shu, Gordon Wetzstein, and Kalyan Sunkavalli. PaletteNeRF: Palette-based Appearance Editing of Neural Radiance Fields, 2023. URL <http://arxiv.org/abs/2212.10699>.

[19] Verica Lazova, Vladimir Guzov, Kyle Olszewski, Sergey Tulyakov, and Gerard Pons-Moll. Control-NeRF: Editable Feature Volumes for Scene Rendering and Manipulation, 2022. URL <http://arxiv.org/abs/2204.10850>.

[20] Boyi Li, Kilian Q. Weinberger, Serge Belongie, Vladlen Koltun, and Rene Ranftl. Language-driven Semantic Segmentation. In *ICLR*, 2022. URL <https://openreview.net/forum?id=RriDjddCLN>.

[21] Hao-Kang Liu, I.-Chao Shen, and Bing-Yu Chen. NeRF-In: Free-Form NeRF Inpainting with RGB-D Priors, 2022. URL <http://arxiv.org/abs/2206.04901>.

[22] Shilong Liu, Zhaoyang Zeng, Tianhe Ren, Feng Li, Hao Zhang, Jie Yang, Chunyuan Li, Jianwei Yang, Hang Su, Jun Zhu, et al. Grounding dino: Marrying dino with grounded pre-training for open-set object detection. *arXiv preprint arXiv:2303.05499*, 2023.

[23] Steven Liu, Xiuming Zhang, Zhoutong Zhang, Richard Zhang, Jun-Yan Zhu, and Bryan Russell. Editing Conditional Radiance Fields. In *2021 IEEE/CVF International Conference on Computer Vision (ICCV)*, pages 5753–5763, 2021. doi: 10.1109/ICCV48922.2021.00572.

[24] Xinhang Liu, Jiaben Chen, Huai Yu, Yu-Wing Tai, and Chi-Keung Tang. Unsupervised Multi-View Object Segmentation Using Radiance Field Propagation. In S. Koyejo, S. Mohamed, A. Agarwal, D. Belgrave, K. Cho, and A. Oh, editors, *Advances in Neural Information Processing Systems*, volume 35, pages 17730–17743, 2022. URL [https://proceedings.neurips.cc/paper\\_files/paper/2022/file/70de9e3948645a1be2de657f14d85c6d-Paper-Conference.pdf](https://proceedings.neurips.cc/paper_files/paper/2022/file/70de9e3948645a1be2de657f14d85c6d-Paper-Conference.pdf).

[25] Aryan Mikaeili, Or Perel, Daniel Cohen-Or, and Ali Mahdavi-Amiri. SKED: Sketch-guided Text-based 3D Editing, 2023. URL <http://arxiv.org/abs/2303.10735>.

[26] Ben Mildenhall, Pratul P. Srinivasan, Rodrigo Ortiz-Cayon, Nima Khademi Kalantari, Ravi Ramamoorthi, Ren Ng, and Abhishek Kar. Local light field fusion: Practical view synthesis with prescriptive sampling guidelines. *ACM Transactions on Graphics (TOG)*, 2019.

[27] Ben Mildenhall, Pratul P. Srinivasan, Matthew Tancik, Jonathan T. Barron, Ravi Ramamoorthi, and Ren Ng. NeRF: Representing Scenes as Neural Radiance Fields for View Synthesis. In *Computer Vision – ECCV 2020: 16th European Conference, Glasgow, UK, August 23–28, 2020, Proceedings, Part I*, pages 405–421, 2020. ISBN 978-3-030-58451-1. doi: 10.1007/978-3-030-58452-8\_24. URL [https://doi.org/10.1007/978-3-030-58452-8\\_24](https://doi.org/10.1007/978-3-030-58452-8_24).

[28] Ashkan Mirzaei, Yash Kant, Jonathan Kelly, and Igor Gilitschenski. LaTeRF: Label and Text Driven Object Radiance Fields. In *Computer Vision – ECCV 2022: 17th European Conference, Tel Aviv, Israel, October 23–27, 2022, Proceedings, Part III*, pages 20–36, 2022. ISBN 978-3-031-20061-8. doi: 10.1007/978-3-031-20062-5\_2. URL [https://doi.org/10.1007/978-3-031-20062-5\\_2](https://doi.org/10.1007/978-3-031-20062-5_2).

[29] Ashkan Mirzaei, Tristan Aumentado-Armstrong, Konstantinos G. Derpanis, Jonathan Kelly, Marcus A. Brubaker, Igor Gilitschenski, and Alex Levinstein. SPIN-NeRF: Multiview Segmentation and Perceptual Inpainting with Neural Radiance Fields, 2023. URL <http://arxiv.org/abs/2211.12254>.

[30] Yicong Peng, Yichao Yan, Shengqi Liu, Yuhao Cheng, Shanyan Guan, Bowen Pan, Guangtao Zhai, and Xiaokang Yang. CageNeRF: Cage-based Neural Radiance Field for Generalized 3D Deformation and Animation. In S. Koyejo, S. Mohamed, A. Agarwal, D. Belgrave, K. Cho, and A. Oh, editors, *Advances in Neural Information Processing Systems*, volume 35, pages 31402–31415, 2022. URL [https://proceedings.neurips.cc/paper\\_files/paper/2022/file/cb78e6b5246b03e0b82b4acc8b11cc21-Paper-Conference.pdf](https://proceedings.neurips.cc/paper_files/paper/2022/file/cb78e6b5246b03e0b82b4acc8b11cc21-Paper-Conference.pdf).

[31] Ben Poole, Ajay Jain, Jonathan T. Barron, and Ben Mildenhall. DreamFusion: Text-to-3D using 2D Diffusion. In *ICLR*, 2023. URL <https://openreview.net/forum?id=FjNys5c7VY>.

[32] Alec Radford, Jong Wook Kim, Chris Hallacy, Aditya Ramesh, Gabriel Goh, Sandhini Agarwal, Girish Sastry, Amanda Askell, Pamela Mishkin, Jack Clark, Gretchen Krueger, and Ilya Sutskever. Learning Transferable Visual Models From Natural Language Supervision. In *Proceedings of the 38th International Conference on Machine Learning*, pages 8748–8763, 2021. URL <https://proceedings.mlr.press/v139/radford21a.html>.

[33] Amit Raj, Srinivas Kaza, Ben Poole, Michael Niemeyer, Nataniel Ruiz, Ben Mildenhall, Shiran Zada, Kfir Aberman, Michael Rubinstein, Jonathan Barron, Yuanzhen Li, and Varun Jampani. DreamBooth3D: Subject-Driven Text-to-3D Generation, 2023. URL <http://arxiv.org/abs/2303.13508>.

[34] Konstantinos Rematas, Ricardo Martin-Brualla, and Vittorio Ferrari. Sharf: Shape-conditioned Radiance Fields from a Single View. In *Proceedings of the 38th International Conference on Machine Learning*, pages 8948–8958, 2021. URL <https://proceedings.mlr.press/v139/rematas21a.html>.

[35] Johannes Lutz Schönberger, True Price, Torsten Sattler, Jan-Michael Frahm, and Marc Pollefeys. A vote-and-verify strategy for fast spatial verification in image retrieval. In *Asian Conference on Computer Vision (ACCV)*, 2016.

[36] Etai Sella, Gal Fiebelman, Peter Hedman, and Hadar Averbuch-Elor. Vox-E: Text-guided Voxel Editing of 3D Objects, 2023. URL <http://arxiv.org/abs/2303.12048>.

[37] Uriel Singer, Shelly Sheynin, Adam Polyak, Oron Ashual, Iurii Makarov, Filippos Kokkinos, Naman Goyal, Andrea Vedaldi, Devi Parikh, Justin Johnson, and Yaniv Taigman. Text-To-4D Dynamic Scene Generation, 2023. URL <http://arxiv.org/abs/2301.11280>.

[38] Roman Suvorov, Elizaveta Logacheva, Anton Mashikhin, Anastasia Remizova, Arsenii Ashukha, Aleksei Silvestrov, Naejin Kong, Harshith Goka, Kiwoong Park, and Victor Lempitsky. Resolution-robust Large Mask Inpainting with Fourier Convolutions. In *2022 IEEE/CVF Winter Conference on Applications of Computer Vision (WACV)*, pages 3172–3182, 2022. doi: 10.1109/WACV51458.2022.00323.

[39] Vadim Tschernezki, Iro Laina, Diane Larlus, and Andrea Vedaldi. Neural Feature Fusion Fields: 3D Distillation of Self-Supervised 2D Image Representations. In *2022 International Conference on 3D Vision (3DV)*, pages 443–453, 2022. doi: 10.1109/3DV57658.2022.00056.

[40] Matthew Wallingford, Aditya Kusupati, Alex Fang, Vivek Ramanujan, Aniruddha Kembhavi, Roozbeh Mottaghi, and Ali Farhadi. Neural Radiance Field Codebooks. In *ICLR*, 2023. URL <https://openreview.net/forum?id=mX56bKDybu5>.

[41] Bing Wang, Lu Chen, and Bo Yang. DM-NeRF: 3D Scene Geometry Decomposition and Manipulation from 2D Images. In *ICLR*, 2023. URL [https://openreview.net/forum?id=C\\_PRLz8bEJx](https://openreview.net/forum?id=C_PRLz8bEJx).

[42] Qianqian Wang, Zhicheng Wang, Kyle Genova, Pratul Srinivasan, Howard Zhou, Jonathan T. Barron, Ricardo Martin-Brualla, Noah Snavely, and Thomas Funkhouser. Ibrnet: Learning multi-view image-based rendering. In *CVPR*, 2021.

[43] Silvan Weder, Guillermo Garcia-Hernando, Aron Monszpart, Marc Pollefeys, Gabriel Brostow, Michael Firman, and Sara Vicente. Removing Objects From Neural Radiance Fields, 2022. URL <http://arxiv.org/abs/2212.11966>.

[44] Qianyi Wu, Xian Liu, Yuedong Chen, Kejie Li, Chuanxia Zheng, Jianfei Cai, and Jianmin Zheng. Object-Compositional Neural Implicit Surfaces. In *Computer Vision – ECCV 2022: 17th European Conference, Tel Aviv, Israel, October 23–27, 2022, Proceedings, Part XXVII*, pages 197–213, 2022. ISBN 978-3-031-19811-3. doi: 10.1007/978-3-031-19812-0\_12. URL [https://doi.org/10.1007/978-3-031-19812-0\\_12](https://doi.org/10.1007/978-3-031-19812-0_12).

[45] Fanbo Xiang, Zexiang Xu, Miloš Hašan, Yannick Hold-Geoffroy, Kalyan Sunkavalli, and Hao Su. NeuTex: Neural Texture Mapping for Volumetric Neural Rendering. In *2021 IEEE/CVF Conference on Computer Vision and Pattern Recognition (CVPR)*, pages 7115–7124, 2021. doi: 10.1109/CVPR46437.2021.00704.

[46] Tianhan Xu and Tatsuya Harada. Deforming Radiance Fields with Cages. In *Computer Vision – ECCV 2022: 17th European Conference, Tel Aviv, Israel, October 23–27, 2022, Proceedings, Part XXXIII*, pages 159–175, 2022. ISBN 978-3-031-19826-7. doi: 10.1007/978-3-031-19827-4\_10. URL [https://doi.org/10.1007/978-3-031-19827-4\\_10](https://doi.org/10.1007/978-3-031-19827-4_10).

[47] Bangbang Yang, Yinda Zhang, Yinghao Xu, Yijin Li, Han Zhou, Hujun Bao, Guofeng Zhang, and Zhaopeng Cui. Learning Object-Compositional Neural Radiance Field for Editable Scene Rendering. In *2021 IEEE/CVF International Conference on Computer Vision (ICCV)*, pages 13759–13768, 2021. doi: 10.1109/ICCV48922.2021.01352.

[48] Bangbang Yang, Chong Bao, Junyi Zeng, Hujun Bao, Yinda Zhang, Zhaopeng Cui, and Guofeng Zhang. NeuMesh: Learning Disentangled Neural Mesh-Based Implicit Field for Geometry and Texture Editing. In *Computer Vision – ECCV 2022: 17th European Conference, Tel Aviv, Israel, October 23–27, 2022, Proceedings, Part XVI*, pages 597–614, 2022. ISBN 978-3-031-19786-4. doi: 10.1007/978-3-031-19787-1\_34. URL [https://doi.org/10.1007/978-3-031-19787-1\\_34](https://doi.org/10.1007/978-3-031-19787-1_34).

[49] Weicai Ye, Shuo Chen, Chong Bao, Hujun Bao, Marc Pollefeys, Zhaopeng Cui, and Guofeng Zhang. IntrinsicNeRF: Learning Intrinsic Neural Radiance Fields for Editable Novel View Synthesis, 2023. URL <http://arxiv.org/abs/2210.00647>.

[50] Hong-Xing Yu, Leonidas Guibas, and Jiajun Wu. Unsupervised Discovery of Object Radiance Fields. In *ICLR*, 2022. URL <https://openreview.net/forum?id=rwE8SshAlxw>.

- [51] Yu-Jie Yuan, Yang-Tian Sun, Yu-Kun Lai, Yuwen Ma, Rongfei Jia, and Lin Gao. NeRF-Editing: Geometry Editing of Neural Radiance Fields. In *2022 IEEE/CVF Conference on Computer Vision and Pattern Recognition (CVPR)*, pages 18332–18343, 2022. doi: 10.1109/CVPR52688.2022.01781.
- [52] Lvmin Zhang and Maneesh Agrawala. Adding Conditional Control to Text-to-Image Diffusion Models, 2023. URL <http://arxiv.org/abs/2302.05543>.
- [53] Richard Zhang, Phillip Isola, Alexei A. Efros, Eli Shechtman, and Oliver Wang. The Unreasonable Effectiveness of Deep Features as a Perceptual Metric. In *2018 IEEE/CVF Conference on Computer Vision and Pattern Recognition*, pages 586–595, 2018. doi: 10.1109/CVPR.2018.00068.
- [54] Shuaifeng Zhi, Tristan Laidlow, Stefan Leutenegger, and Andrew J. Davison. In-Place Scene Labelling and Understanding with Implicit Scene Representation. In *2021 IEEE/CVF International Conference on Computer Vision (ICCV)*, pages 15818–15827, 2021. doi: 10.1109/ICCV48922.2021.01554.
- [55] Tianfei Zhou, Fatih Porikli, David J. Crandall, Luc Van Gool, and Wenguan Wang. A survey on deep learning technique for video segmentation. *IEEE Transactions on Pattern Analysis and Machine Intelligence*, 45(6):7099–7122, 2023. doi: 10.1109/TPAMI.2022.3225573.
- [56] Zhizhuo Zhou and Shubham Tulsiani. SparseFusion: Distilling View-conditioned Diffusion for 3D Reconstruction, 2023. URL <http://arxiv.org/abs/2212.00792>.
- [57] Jingsen Zhu, Yuchi Huo, Qi Ye, Fujun Luan, Jifan Li, Dianbing Xi, Lisha Wang, Rui Tang, Wei Hua, Hujun Bao, and Rui Wang. I $\hat{S}$ -SDF: Intrinsic Indoor Scene Reconstruction and Editing via Raytracing in Neural SDFs, 2023. URL <http://arxiv.org/abs/2303.07634>.